Renewable Energy 212 (2023) 350–358

Contents lists available at ScienceDirect

Renewable Energy

journal homepage: www.elsevier.com/locate/renene

Numerical simulation of biogas chemical looping reforming in a dual fluidized bed reactor

Giuseppe Cristian Piso [a], Piero Bareschino [a,*], Paola Brachi [b], Claudio Tregambi [a], Giovanna Ruoppolo [b], Francesco Pepe [a], Erasmo Mancusi [a]

[a] Dipartimento di Ingegneria, Università degli Studi del Sannio, P.zza Roma 21, Benevento, Italy
[b] Istituto di Scienze e Tecnologie per l'Energia e la Mobilità Sostenibili, Consiglio Nazionale Delle Ricerche (STEMS-CNR), P.le V. Tecchio 80, Napoli, Italy

ARTICLE INFO

Keywords:
Biogas
Chemical looping reforming
Syngas
Bioenergy with carbon capture and storage
Autothermal reforming
Carbon fouling

ABSTRACT

Conversion technologies with low environmental impact and high energetic efficiency are needed to ensure clean, efficient, and cost-effective exploitation of renewable carbonaceous fuels like biogas. In the present study, the Chemical Looping Reforming of biogas is proposed and numerically investigated to pursue this goal. Preliminarily, a thermodynamic model was implemented by means of the Aspen Plus® commercial software to identify the conditions where carbon formation and deposition do not occur. A simple hydrodynamic model of a Dual Fluidized Bed reactor coupled with a 1D, static, and isothermal kinetic model was adopted. The effects of variations in biogas composition (namely, CH_4:CO_2 ratio and water content) and in other relevant process parameters (e.g., the oxygen-to-fuel ratio and FR operating temperature) on the process performances in terms of the reactants conversion degree, syngas yield, and syngas composition were assessed and critically discussed. Very high conversion degree for both CH_4 (93%) and CO_2 (87%), as well as syngas yield ranging up to 3.74, were evaluated.

1. Introduction

To achieve climate neutrality by 2050, the European Commission expects EU members to reduce carbon dioxide emissions into atmosphere by at least 55% with respect to 1990 levels by 2030 [1]. To reach this target, fossil fuels must be progressively replaced by renewable energy resources. Among the latter, biomass plays a key role as a source of renewable carbon and hydrogen through different pathways. Biomass anaerobic digestion, *i.e.* the decomposition of organic matter by bacterial action to produce biogas and digestate, has received considerable attention in recent years since its total energy request is lower than that of other thermochemical conversion processes [2]. In addition, the total carbon dioxide emissions of the process are such as to be compensated by the CO_2 absorbed during the biomass life cycle, keeping net emissions close to zero [2].

Depending on the kind of biomass fed to the digestor, biogas mainly contains methane (55–65%), carbon dioxide (35–45%), trace of hydrogen sulphide, hydrogen, ammonia, nitrogen, and it is saturated with water vapor [3]. Therefore, prior to use, biogas must undergo purification and upgrading treatments in order to remove the undesired compounds that can compromise its distribution and downstream utilization. The main use of simply purified biogas is related to its combustion in combined heat and power (CHP) generators, albeit the total system efficiency is penalized by the high CO_2 content [4]. To increase both methane content and calorific value of purified biogas, the carbon dioxide has to be removed in the upgrading phase. To this aim, literature suggests several methods, both biological and physicochemical, with the latter being actively used on commercial scale (TRL 9) [1,2,5]; but, in order to minimize the carbon footprint of the whole process storage (CCS) or utilization (CCU) of separated CO_2 must be considered. In this context, study by Ref. [6], which deal with the migration of new biogas upgrading plants from centralized/large-to decentralized/small-scale, indicate that CCU is more advisable than CCS [7]. Besides being used as fuel, simply purified biogas can be reformed to produce a syngas classified as a green product [8].

Today, catalytic steam methane reforming (SRM) is the most common process used to convert CH_4 into syngas; but, due to the highly endothermic reaction involved, it is a high energy demand process that requires heating of the reactor by external combustion, with the consequent release of significant CO_2 emissions (≈7 kg_{CO2}/kg_{H2}) [9]. An

* Corresponding author.
E-mail address: piero.bareschino@unisannio.it (P. Bareschino).

https://doi.org/10.1016/j.renene.2023.05.060
Received 9 January 2023; Received in revised form 4 May 2023; Accepted 13 May 2023
Available online 16 May 2023

attractive alternative to SMR, is the autothermal reforming (ATR) process, where methane and steam are mixed with oxygen so that the exothermic methane partial oxidation occur, thus providing the heat for endothermic steam reforming reaction and ideally avoiding the need of an external energy supply. However, heat management could pose a serious challenge and an air separation unit (ASU) is required to supply pure oxygen to the system [10].

Autothermal Chemical Looping Reforming (a-CLR) is based on two interconnected reactors, i.e., the air reactor (AR), in which an oxygen carrier (OC) is oxidized undergoing an increase in its temperature, and the fuel reactor (FR), where the OC, apart from transferring oxygen, acts both as a thermal vector and a reforming catalyst. Consequently, neither an ASU nor external heater are required. The most common CLR configuration consists of a dual fluidized bed reactor system with a bubbling bed serving as fuel reactor (FR) and a riser as air reactor (AR), connected via a loop-seal system for avoiding the mixing of the feed gases and a cyclone for the particle separation [11]. Different oxygen-carriers have been tested in literature, although Ni-based oxygen-carriers represent the most widely used having a long lifetime and no noticeable reactivity changes over time [12].

Several authors have investigated the performances of CLR systems. In a 140-kW pilot plant [13], Pröll et al. showed that at low global air/fuel ratios the conversion approaches to thermodynamic equilibrium, with the system performance depending on the steam amount needed to prevent carbon deposition. Rydén et al. [14] reported that by adding 25%$_{vol}$ of steam to methane there is no accumulation of carbon deposits and the composition of the reformer gas is very close to the thermodynamical equilibrium one. Later, the same authors [15] demonstrated that by substituting the steam with CO_2 the formation of solid carbon is quite negligible. Ortiz et al. [16] showed that the oxygen carrier circulation rate (NiO/CH_4 molar ratio) affects the system performance, reporting that a $NiO_{reacted}/CH_4$ molar ratio close to 1 is needed to maximize the hydrogen production; however, this molar ratio is lower than that required to ensure autothermal operation (about 1.25).

In all the above-mentioned papers, methane was considered as a fuel, its conversion is at or close to the equilibrium, and carbon formation and deposition is negligible. Consequently, this suggests that considering a less valuable fuel such as biogas in a CLR system is worth investigating.

Given the high content of carbon dioxide in biogas, dry reforming CH_4 reaction occurs along with steam reforming and partial oxidation in a process known as tri-reforming [17], as summarized in Table 1.

Literature presents a number of studies on the influence of several parameters on biogas reforming processes, most of them having the limitation of just considering thermodynamic equilibrium conditions [18–21]. Furthermore, to the best of authors' knowledge, there is no literature directly dealing with biogas CLR while there are a number of preliminary studies on biogas utilization as a fuel in Chemical Looping Combustion (CLC) processes. More specifically, biogas CLC was assessed by Hoteit et al. [22] in a batch fluidized bed reactor, and later demonstrated in a CLC unit using a CuMn-based [23] oxygen carrier. More recently, Cabello et al. [24] performed a techno-economic analysis of a Chemical Looping Combustion process for biogas generated from livestock farming and agro-industrial waste. Their data showed that CLC can be a competitive and sustainable option if captured CO_2 was used. On the other hand, Kong et al. [25] proposed an iron-based chemical looping technology (namely, a Chemical Looping Water Splitting) as an alternative pathway for biogas to syngas conversion. Such a process exhibited a great level of process intensification, requiring neither upstream biogas comprehension and purification, nor downstream CO_2 removal and H_2 separation. Nevertheless, direct biogas CLR has not been thoroughly investigated so far, in particular focusing on the quantitative influence of the operating parameters on the process performances. Consequently, in the present work a CLR system has been numerically investigated considering biogas as a feedstock and Ni/γ-Al_2O_3 as an oxygen carrier. The CO_2 content in the feed makes the process more energy intensive as dry reforming is more endothermic than steam reforming, but the conversion of the biogas CO_2 content, as previously mentioned, allows to make the balance of its emission in atmosphere negative.

Table 1
tri-reforming reaction.

Methane steam reforming	$CH_4 + H_2O \leftrightarrow 3H_2 + CO$
Methane partial oxidation	$CH_4 + \frac{1}{2}O_2 \leftrightarrow 2H_2 + CO$
Methane dry reforming	$CH_4 + CO_2 \leftrightarrow 2H_2 + 2CO$

2. Materials and methods

The proposed DFB system is schematically shown in Fig. 1. In detail, the bubbling fluidized bed serving as fuel reactor is divided into two zone along its height, namely: i.) the dense zone, which includes the solid material and extends from the bottom of the bed up to the height of the weir (the dark grey area of FR in Fig. 1) and ii.) the freeboard, in the upper part (the white area of FR in Fig. 1), where only gaseous streams are present. The solid above the weir is conveyed to the loop-seal through a pipe and fed to the air reactor (AR) to be oxidized. The loop-seal allows the circulation of the solid from the FR to the base of the AR, thus preventing the direct contact of gas streams from the two

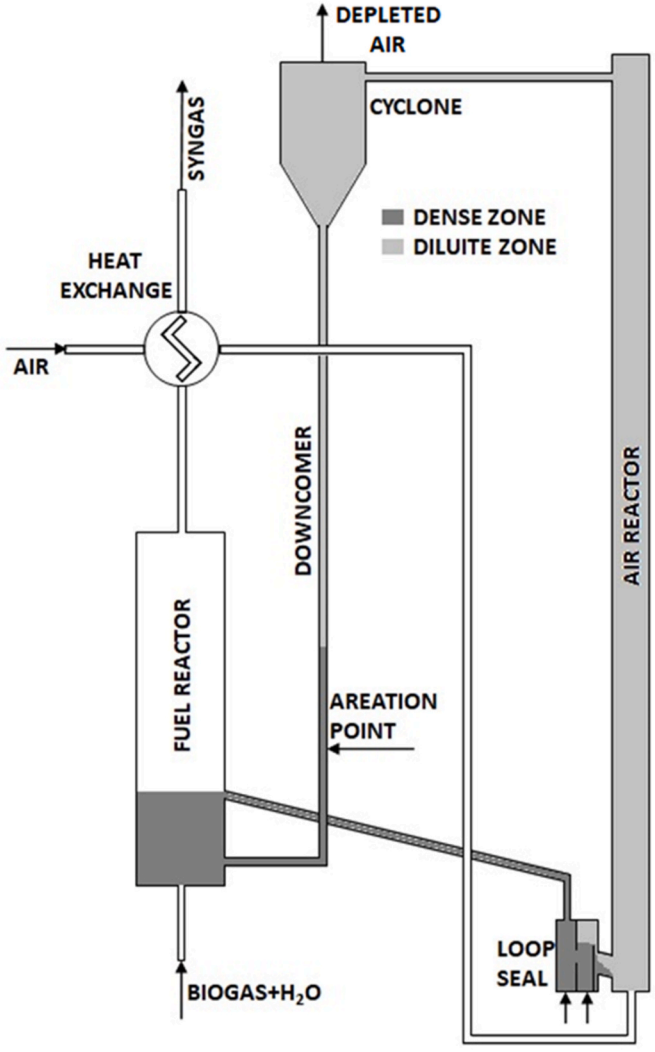

Fig. 1. Conceptual scheme of DFB system [26].

sections of the system. The air reactor is a riser in which pneumatic conveying conditions are established. Before being fed to the reactor, the airflow is preheated in a counterflow heat exchanger using the sensible heat of the outlet gas from the FR. At the top of AR, the separation of the gas (nitrogen and unreacted oxygen) from the solid particles occurs in a cyclone. Finally, the solid particles are fed to the fuel reactor trough a system composed by a downcomer and a L-valve. More details on the considered system can be found in Ref. [26].

The system is developed by matching a simple hydrodynamic model with a 1D static and isothermal kinetic model and formulated with the aim to find out temperature, solids conversion degree, and gaseous species concentration at the exit of both Fuel and Air reactors.

The hydrodynamic model is based on the simultaneous solution of the units shown in Fig. 1, namely riser, cyclone, downcomer, L-valve, BFB and loop-seal. The governing laws defining each unit and the related interconnections are reported in the supplementary material. Given the total amount of solid in the system, the pressure at the outlet of the cyclone and the BFB, the fluidization gas flow rates in both the riser and the BFB, and the aeration gas flow rates in both the L-Valve and the loop-seal, the initial solid distribution was calculated. Based on this initial condition, the dynamic model was consequently solved to assess the solid circulation rate at the steady state. More details on the hydrodynamic model.

The kinetic model considered is based on a previous work [26]. Table 2 reports the reactive scheme and the enthalpy change associated with each of the reactions occurring in the system. The reaction rates and kinetic constants of kinetic model are taken from Refs. [27,28].

In the AR, considered adiabatic, Ni is oxidized to NiO through the reaction R1 (Table 2). In the FR freeboard, only the homogenous water gas shift reaction is taken into account since the extents of the uncatalyzed steam and dry reforming reactions are negligible. The FR is assumed to work as an isothermal reactor, with part of the needed thermal energy provided by the Ni exothermic oxidation reaction that occurs in the AR. When not enough, an external thermal integration to this latter is considered.

The complete numerical model (hydrodynamic and kinetic) is solved by using the commercial software package COMSOL Multiphysics®. A detailed description of the model and its assumptions, as well as the solution procedure, is provided in the supplementary material and further details can be found in Ref. [26]. It should be noted that in a CLR process, the oxygen-to-fuel ratio must be kept as low as possible to avoid complete oxidation of the fuel [7]. This can be accomplished either by varying the air-to-fuel ratio (namely, by reducing the air flow rate to the AR so to oxidize the OC only partially in the air reactor) or by regulating the solids circulation rate (i.e., by increasing the air flow rate to the AR over the value corresponding to a fully oxidized OC at the exit of the air reactor). In the present work, the latter approach was adopted to ensure that the AR always works in dilute transport regime.

Table 3 reports the operating conditions, the geometrical characteristics, and the physical parameters of solid bed materials for the DFB system for the base case. The total solid inventory in the system was calculated by considering a 15% excess with respect to the minimum amount required for the proper operation of the loop-seal, the downcomer, and the L-valve.

Finally, the syngas yield η_S and the overall thermal efficiency $\eta_{Th,O}$ of the process were evaluated, respectively, as:

$$\eta_s = \frac{F_{H_2} + F_{co}}{F_{CH_4}} \tag{1}$$

$$\eta_{Th,O} = \frac{F_{H_2} LHV_{H_2} + F_{CO} LHV_{co}}{F_{CH_4} LHV_{CH_4} + Q_s} \tag{2}$$

where F_i is the molar flow rate and LHV_i the lower heating value of the ith specie and Q_s the thermal integration to isothermically operate the FR.

Table 2
Reactive scheme and related enthalpy variations.

Oxygen carrier oxidation reaction			
OC oxidation	$2Ni + O_2 \rightarrow 2NiO$	$\Delta H = -468 \frac{kJ}{mol_{O_2}}$	R1
Oxygen carrier reduction reactions			
Methane oxidation	$CH_4 + 2NiO \leftrightarrow 2Ni + 2H_2 + CO_2$	$\Delta H = 162 \frac{kJ}{mol_{CH_4}}$	R2
Hydrogen oxidation	$H_2 + NiO \leftrightarrow Ni + H_2O$	$\Delta H = -16 \frac{kJ}{mol_{H_2}}$	R3
Carbon monoxide oxidation	$CO + NiO \leftrightarrow Ni + CO_2$	$\Delta H = -49 \frac{kJ}{mol_{CO}}$	R4
Methane partial oxidation	$CH_4 + NiO \leftrightarrow Ni + 2H_2 + CO$	$\Delta H = 211 \frac{kJ}{mol_{CH_4}}$	R5
Reduction reactions catalyzed by Ni			
Methane steam reforming	$CH_4 + H_2O \xleftrightarrow{Ni} 3H_2 + CO$	$\Delta H = 227 \frac{kJ}{mol_{CH_4}}$	R6
Methane dry reforming	$CH_4 + CO_2 \xleftrightarrow{Ni} 2H_2 + 2CO$	$\Delta H = 259 \frac{kJ}{mol_{CH_4}}$	R7
Water gas shift	$CO + H_2O \xleftrightarrow{Ni} H_2 + CO_2$	$\Delta H = -33 \frac{kJ}{mol_{CO}}$	R8
Methane decomposition	$CH_4 \xleftrightarrow{Ni} C + 2H_2$	$\Delta H = 91 \frac{kJ}{mol_{CH_4}}$	R9
Carbon gasification by steam	$C + H_2O \xleftrightarrow{Ni} H_2 + CO$	$\Delta H = 136 \frac{kJ}{mol_{H_2O}}$	R10
Carbon gasification by CO_2	$C + CO_2 \xleftrightarrow{Ni} 2CO$	$\Delta H = 169 \frac{kJ}{mol_{CO_2}}$	R11

3. Results and discussion

Preliminary thermodynamic calculations were carried out by minimizing the Gibbs free energy of the system. This allowed not only to select values of temperature and pressure more suitable to promote the reactants conversion and prevent the side reactions, but also to evaluate the influence of the CH_4:CO_2 ratio and the water content on the equilibrium gaseous compositions at the exit of the FR and the solid carbon formation and deposition.

3.1. Thermodynamic analysis

Thermodynamic analysis was performed in Aspen Plus® by using the R-Gibbs reactor and assuming the ideal gas law to describe the behaviour of gaseous phase. The model involves two inlets, one containing only the fully oxidized oxygen carrier and the other made up of a CH_4, CO_2, and H_2O mixture, and two outlet streams, one for the solids (including solid carbon) and the other for gaseous species.

Fig. 2 reports the equilibrium molar fractions of solid carbon and gaseous species as a function of either temperature or pressure, for a

Table 3
Operating conditions, properties of bed material and geometrical characteristics of DFB for the base case.

Operating conditions		Geometrical characteristics		Properties of bed material	
$W[kg\,s^{-1}]$	0.0023	$D_R[m]$	0.102	$\rho_p[kg\,m^{-3}]$	2540
$U_B[m\,s^{-1}]$	0.2	$h_R[m]$	5.6	$d_p[m]$	$2.55{\cdot}10^{-4}$
$U_R[m\,s^{-1}]$	3.3	$h_B[m]$	2	$\varepsilon_{mf}[-]$	0.445
$Q_{LV}[m^3 s^{-1}]$	$5.5{\cdot}10^{-5}$	$h_w[m]$	0.3	$\varepsilon_{BFB}[-]$	0.445
$G_S[kg\,m^{-2}s^{-1}]$	0.2	$D_B[m]$	0.12	$m_{inv}[kg]$	11.6

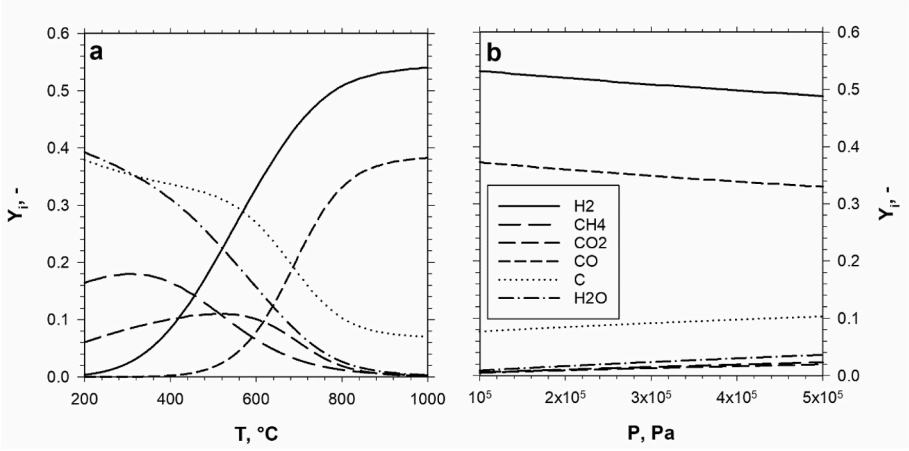

Fig. 2. Equilibrium molar fraction for CH_4:CO_2 = 3:2 as a function of operating T and P for a given value of P (a) and T(b).

given value of P (Fig. 2a) or T (Fig. 2b), when no water steam is considered. Data show that an increase in the operating temperature favours the biogas conversion and the syngas yield for any given pressure, as shown in Fig. 3a. Conversely, both biogas conversion and syngas yield decrease with an increase in the operating pressure (Fig. 3b) for any given temperature. It should be noted that, whatever the operating conditions considered, the formation of solid carbon occurs. Although carbon deposition does not pose a serious threat in CLR process since carbon deposits can be easily burnt in the AR by exploiting its energy content [29], the addition of water is required to avoid its formation in the FR. Moreover, since carbon formation is strictly connected to the CH_4:CO_2 ratio in biogas, the effects of both steam addition and CH_4:CO_2 ratio on carbon formation and deposition will be briefly discussed.

Regions where carbon formation occurs are reported in Fig. 3, in both the (T, Y_{H2O}) and the (T, CH_4:CO_2) space phase.

The analysis of the surface morphology of the two plots shows interesting results. Below each curve in Fig. 3a, *i.e.*, for a given CH_4:CO_2 ratio, carbon formation occurs whatever the operating temperature and the water steam molar fraction. The same is true above each curve in Fig. 3b, *i.e.*, for any given Y_{H2O}, whatever the methane-to-carbon dioxide ratio and the operating temperature. Consequently, it is mandatory to vary the steam-to-carbon or the oxygen-to-carbon ratio to avoid coke formation and deposition.

Given all of the above, an operating pressure equals to 10^5 Pa, a fed molar composition CH_4:CO_2:H_2O ratio equals to 24:16:1 and FR operating temperature equals to 900 °C were selected as base case values, as summarized in Table 4.

Table 4
Additional operating conditions for the base case.

Operating conditions	
$P[Pa]$	10^5
$T[°C]$	900
$Y_{CH_4}[-]$	0.48
$Y_{CO_2}[-]$	0.32
$Y_{H_2O}[-]$	0.20

3.2. Performance analysis

To highlight the effects of a variation in the operating conditions reported in Table 4, on the process performance in terms of CH_4 and CO_2 conversion degree and produced gas composition (i.e., components molar fractions and H_2:CO ratio), a parametric analysis was carried out as described in the following. The impact of a change in the oxygen-to-fuel ratio was also assessed. It should be noted that the OC conversion degree was higher than 99% in all the considered conditions.

3.2.1. Influence of T_{FR}

The effects of a variation in the FR operating temperature on the gas composition at the fuel reactor exit are reported in Fig. 4. It results that, increasing the T_{FR}, H_2 and CO molar fractions slightly increase, while Y_{CH4}, Y_{H2O}, and Y_{CO2} a little decrease. However, whatever the considered T_{FR}, gas molar fractions at the exit of the FR are close to thermodynamic equilibrium.

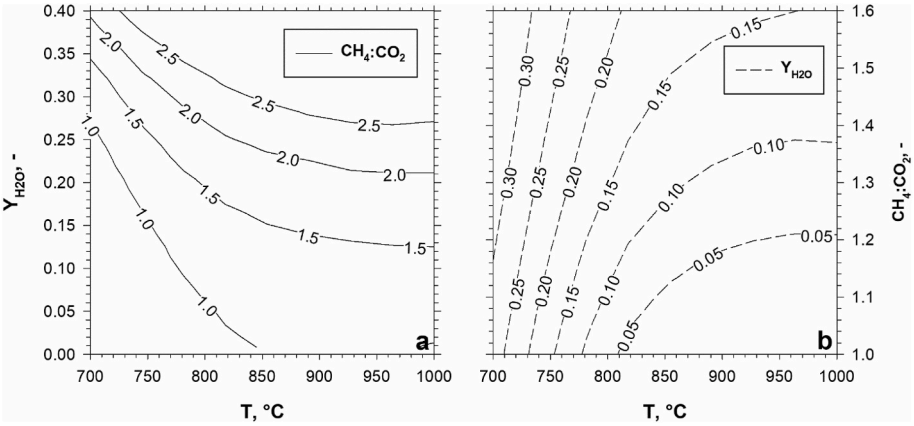

Fig. 3. Carbon formation regions as a function of operating temperature T, H_2O molar fraction (a) and CH_4:CO_2 ratio (b) parametric in CH_4:CO_2 ratio and Y_{H2O}, respectively.

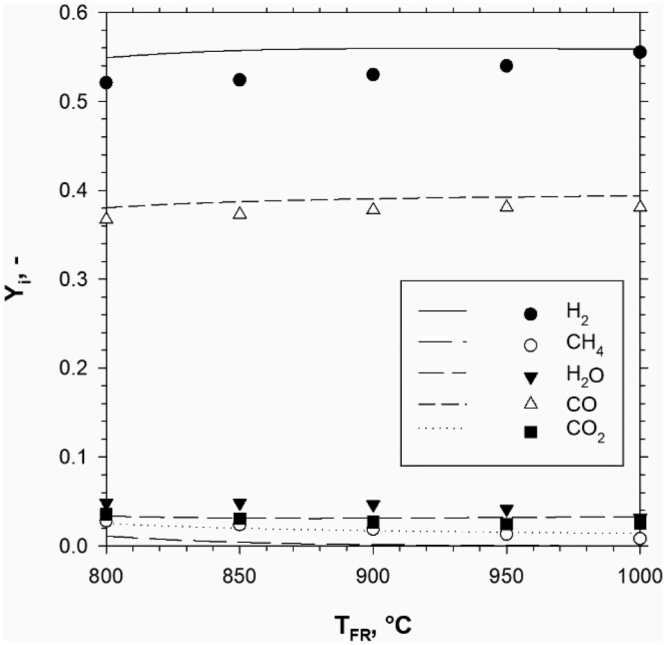

Fig. 4. Calculated (dots) and equilibrium (lines) gas molar fractions at the exit of the FR as function of temperature.

Fig. 5 reports CH_4 and CO_2 conversion degree (Fig. 5a) and H_2:CO syngas ratio, *SR* (Fig. 5b), as a function of FR operating temperature. Noteworthy, *SR* decreases as T_{FR} increases and reaches a minimum at 900 °C. This behaviour is due to the activation of homogenous WGS reaction (R8) in the freeboard of the FR. Although high temperatures favour the reverse WGS reaction, the concentration of water steam being higher than that of carbon dioxide shifts the reaction towards the direct direction. The combined effect of an increase in T_{FR} on both the endothermic reactions and the activation of R8 is clearly visible in Fig. 5a: the conversion of methane increases steadily with the temperature, while the conversion of carbon dioxide slows down to decrease above 950 °C. As a consequence, more H_2 than CO is produced and the *SR* increases as the FR operating temperature exceeds 900 °C.

Operating at a higher temperature is optimal to maximize methane conversion and reducing coke formation. However, high temperatures constitute a rather severe condition from the catalyst stability standpoint; in addition, the thermal power required for the isothermal operation of the FR increases with T_{FR} as reported by Ref. [30]. The presence of CO_2 in the FR feed makes the system even more energy intensive. Altogether, it can be concluded that assuming an operating temperature of 900 °C for the FR represents a good compromise between the two aspects mentioned above.

3.2.2. Influence of oxygen-to-fuel ratio

Changing the height of the weir, while keeping constant the fluidization gas velocity in the FR, results in a variation not only in the gas phase residence time but also in the oxygen-to-fuel ratio. Actually, increasing h_W results in the rise of the FR solid inventory and this, in turn, decreases the circulating solid flow rate, so that the oxygen transported from the AR to the FR by OC decreases too. This results in an increase in both the hydrogen and carbon monoxide molar fractions, as shown in Fig. 6a, as well as in the rise of the CH_4 and CO_2 conversion degree (Fig. 6b). The syngas H_2:CO ratio was close to 1.4, whatever the weir height considered.

Changing the FR diameter, while keeping constant the fluidization gas velocity in the fuel reactor, ensures a variation in oxygen-to-fuel ratio, but keeps the gas residence time unchanged. However, it should be noted that the solid inventory in the FR changes as the square of D_B, while it varies linearly with h_W. The resulting noticeable decrease in the circulating solid flow rate leads to a lower oxygen concentration available in the FR. The reaction rates of non-catalytic reduction reactions (R2-R5) consequently decrease and, hence, a lower conversion degree of CH_4 and a higher conversion degree of CO_2, with respect to the base case, were detected as D_B increases (Fig. 7b). The SR was 1.4 whatever the considered reactor diameter.

Finally, the effect of the change in oxygen-to-fuel ratio caused by a variation in the circulating solids mass flux (G_S), was also taken into account. As a matter of the fact, the NiO-to-CH_4 ratio increases with the OC circulation rate in the FR, as well as the reaction rates of non-catalytic reduction reactions (R2-R5). Consequently, more and more CO_2 and H_2O are produced as G_S increases (Fig. 8a). In terms of conversion degree (Fig. 8b), although X_{CH4} approaches 1 as the circulating solids mass flux increases, an abrupt reduction in X_{CO2} can be observed.

3.2.3. Influence of steam-to-carbon ratio

In order to assess the effects of a variation in the steam-to-carbon ratio, it was considered the change in the steam content with respect to the base case, while keeping the CH_4:CO_2 ratio constant. Fig. 9 reports the gas molar fractions Y_i at the exit of the FR (Fig. 9a), the CH_4 and CO_2 conversion degree X_i (Fig. 9b), and the H_2:CO syngas ratio *SR* (Fig. 9c) as a function of Y_{H2O}. Data show that increasing the steam content in the feed results in a rise of the methane conversion degree (Fig. 9b) *via* steam methane reforming reaction (R6). At the same time, X_{CO2} decreases since R6 prevails over dry methane reforming. Both H_2 and CO molar fractions decreases (Fig. 9a), but to a different extent, given that the R6 reaction produces three times more hydrogen than carbon monoxide. Finally, by doubling the water molar fraction, the *SR* goes

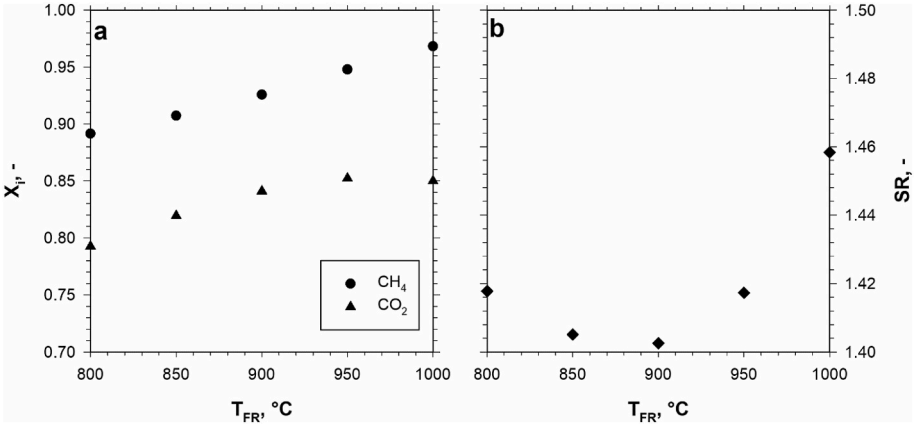

Fig. 5. CH_4 and CO_2 conversion degree (a) and H_2:CO syngas ratio (b) as a function of FR operating temperature.

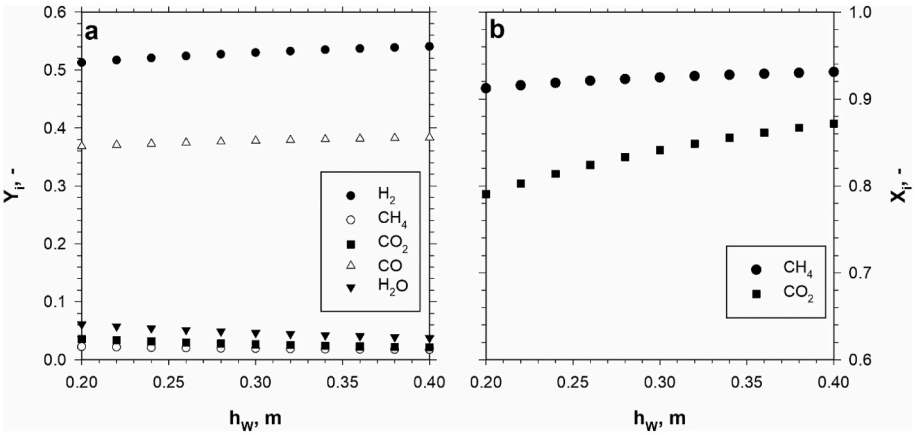

Fig. 6. Gas molar fractions (a) and conversion degrees (b) as a function of weir height.

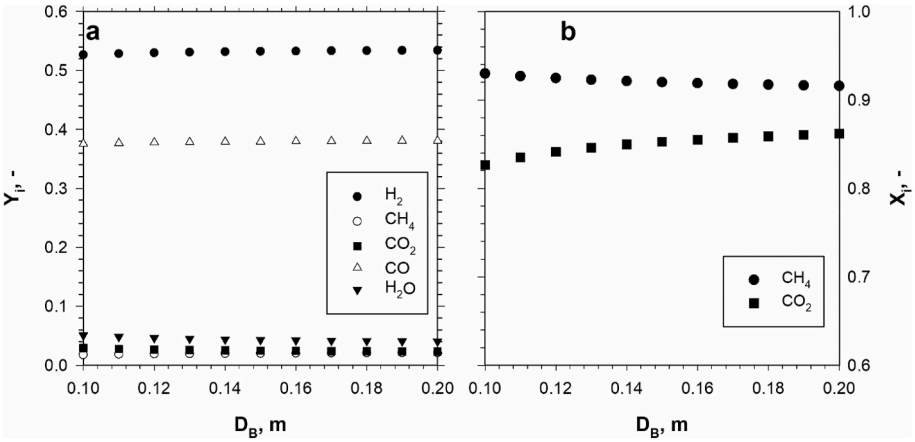

Fig. 7. Gas molar fractions (a) and conversion degrees (b) as a function of fuel reactor diameter D_B.

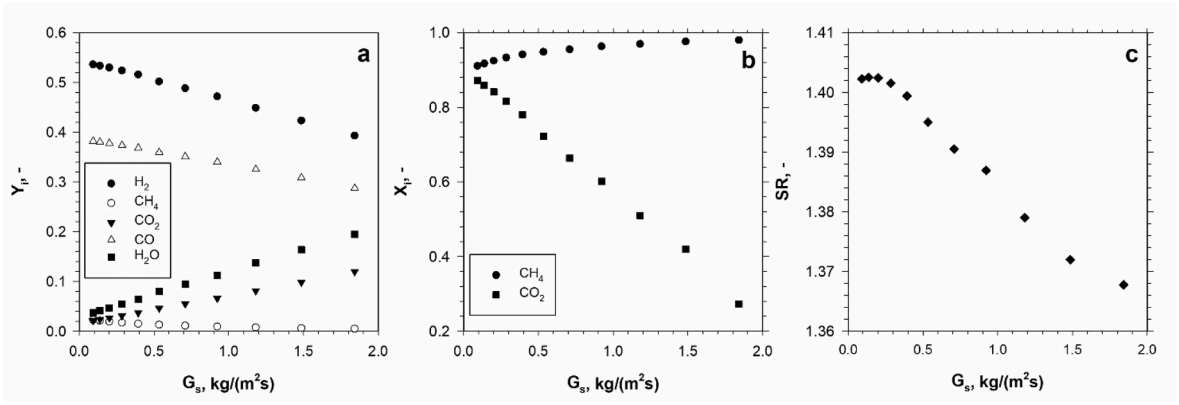

Fig. 8. Gas molar fractions (a), conversion degrees (b), and *SR* (c) as a function of circulating solid mass flux G_S.

from 1.4 to about 1.8 (Fig. 9c). The proposed rationale is supported by the finding that the thermal power needed to endure isothermal operation of the FR decreases as the water content in the feed increases, given the less endothermicity of the steam reforming reaction (R6) over the dry reforming one (R7). Since having high X_{CO2} at the exit makes carbon dioxide emissions negative for the proposed process, the adoption of a low steam-to-carbon ratio maximizes the CO_2 conversion degree, whatever the operating condition considered, while minimizing the *SR*.

For a fixed $Y_{H2O} = 0.20$ in the feed, different CH_4:CO_2 ratios in the range 1:1 ÷ 5:3 were considered. Fig. 10 reports gas molar fractions Y_i at the exit of the FR (Fig. 10a), the CH_4 and CO_2 conversion degrees X_i (Fig. 10b), and the H_2:CO syngas ratio *SR* (Fig. 10c) as a function of CH_4:CO_2 ratio. It results that increasing the methane over carbon dioxide content in the feed increases the hydrogen molar fraction with small variations in Y_{CO}, whereas both Y_{H2O} and Y_{CO2} decreases (Fig. 10a), Accordingly, methane conversion degree decreases, while that of carbon dioxide increases (Fig. 10b). The syngas ratio grows linearly as the methane content in the FR fed increases (Fig. 10c). The required thermal power also increases since more methane must be catalytically

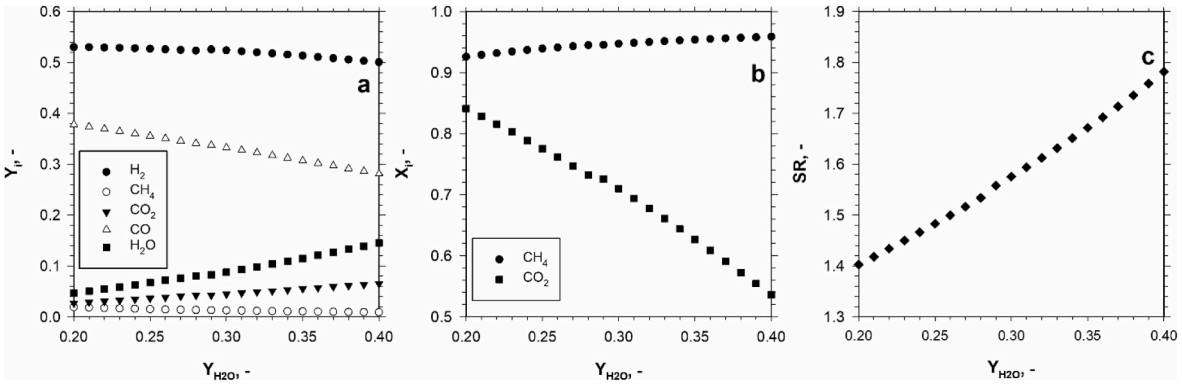

Fig. 9. Gas molar fractions (a), conversion degrees (b), and syngas H_2:CO ratio (c) as a function of H_2O molar fraction. CH_4:CO_2 = 3:2.

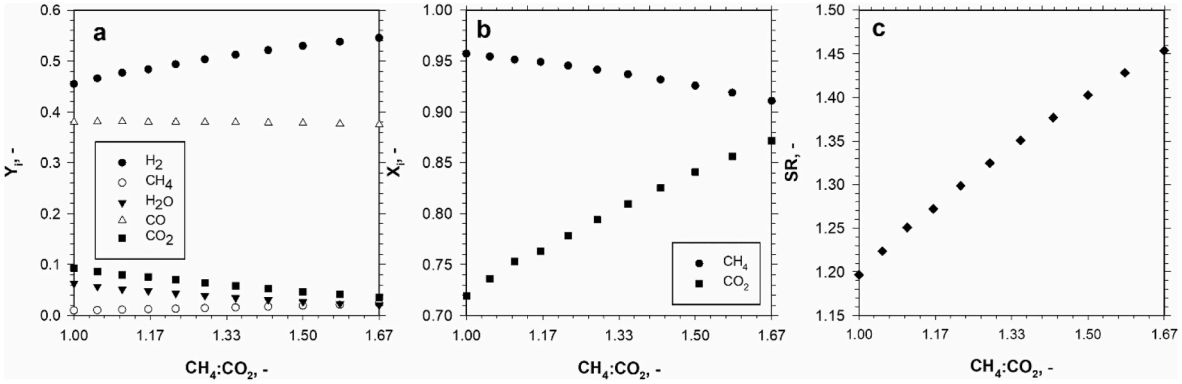

Fig. 10. Gas molar fractions (a), conversion degrees (b), and syngas H_2:CO ratio (c) as a function of CH_4:CO_2 ratio. Y_{H2O} = 0.2.

converted by the endothermic reactions (R2, R5-R7).

As a final point, the syngas yield and the overall thermal efficiency were evaluated according to Eq.s (1) and (2) for the investigated operating conditions. Calculated values are reported in Table 5.

Table 5
Syngas yield and overall thermal efficiency for different values of investigated parameters. All the other operating conditions are those reported in Tables 3 and 4

	η_S [−]	$\eta_{Th,O}$ [−]
T_{FR} [°C]		
800	3.43	0.52
850	3.50	0.52
900	3.58	0.52
950	3.67	0.53
1000	3.73	0.53
h_W [m]		
0.2	3.44	0.51
0.3	3.58	0.52
0.4	3.68	0.53
D_B [m]		
0.1	3.56	0.52
0.15	3.60	0.53
0.2	3.61	0.53
G_s [kg/(m^{2}s)]		
0.09	3.63	0.53
0.92	3.26	0.49
1.84	2.74	0.43
Y_{H2O} [−]		
0.2	3.58	0.52
0.3	3.64	0.53
0.4	3.72	0.53
CH_4:CO_2 [-]		
1:1	3.74	0.53
3:2	3.58	0.52
5:3	3.52	0.52

Syngas yield ranges from 2.74 up to 3.74. The lowest η_S value is reached when the highest circulating solids mass flux is considered, consistently with the production of more and more CO_2 and H_2O (instead of CO and H_2) assessed with increasing G_S values. Under the same operating conditions, the lowest overall thermal efficiency value was evaluated too. The highest syngas yield was assessed when a CH_4:CO_2 ratio equal to 1 in the feed was considered. Correspondingly, a $\eta_{Th,O}$ value of 0.53 was calculated.

4. Conclusion

In this work, the CLR of biogas to syngas in a dual circulating fluidized bed reactor was proposed and numerically investigated. The main findings of the simulations based on the purpose-built coupled kinetic and hydrodynamic model as well as that from the ancillary carried out thermodynamic analysis can be summarized as follows. The process performances, in terms of biogas conversion and SR, are weakly influenced by the Fuel Reactor temperature over the range of values investigated (800 °C–1000 °C), whereas a strong dependence on the composition of the reagent mixture is observed.

The increase in the feed water content promotes the steam over the dry reforming reaction, therefore the thermal power needed to ensure isothermal operation of the FR decreases; at the same time, the conversion of carbon dioxide decreases, while the SR increases. The hydrogen yield moves from 2.1 to 2.37 for a steam-to-carbon ratio increasing from 0.9 to 2.4. Likewise, it results that a variation in the biogas methane-to-carbon dioxide ratio (CH_4:CO_2) from 1:1 to 5:3, at a fixed water fraction into the reactant mixture, results in an increase in the hydrogen molar fraction, while the CO fraction stays substantially constant. At the same time, the conversion of methane decreases slightly, but remains equal to 90%, while that of carbon dioxide

increases. Depending on biogas CH_4:CO_2 ratio and the amount of steam fed, it is possible to obtain a syngas with a H_2:CO ratio variable between 1.2 and 1.8. This, in turn, makes the proposed process suitable to provide an intermediate exploitable in many industrial applications, such as the oxo-synthesis or hydroformylation (H_2:CO = 1:1), the dimethyl ether production (H_2:CO = 1:1), and the acetic acid synthesis (H_2:CO = 1:1). The upgrading of the obtained syngas to higher *SR* ratios in a separate water gas shift process is, instead, required for the synthesis of Fischer-Tropsch transportation fuels (H_2:CO = 2:1) and methanol (H_2:CO = 2:1).

Finally, results highlighted that very high conversion degree for both methane (93%) and carbon dioxide (87%) can be achieved by suitably setting the geometry of the FR.

Overall, the results of this study suggest that biogas is not only suitable for direct conversion into syngas, but can be an important precursory of a wide variety of valuable chemical intermediates/end-products.

CRediT authorship contribution statement

Giuseppe Cristian Piso: Investigation, Visualization, Writing – original draft, Writing – review & editing. **Piero Bareschino:** Conceptualization, Software, Visualization, Writing – original draft, Writing – review & editing, Supervision. **Paola Brachi:** Investigation, Visualization, Writing – original draft, Writing – review & editing. **Claudio Tregambi:** Writing – original draft. **Giovanna Ruoppolo:** Conceptualization, Investigation, Writing – original draft, Writing – review & editing. **Francesco Pepe:** Writing – original draft, Writing – review & editing. **Erasmo Mancusi:** Conceptualization, Software, Visualization, Writing – original draft, Writing – review & editing.

Declaration of competing interest

The authors declare that they have no known competing financial interests or personal relationships that could have appeared to influence the work reported in this paper.

Data availability

Data will be made available on request.

Acknowledgement

The article is based on a manuscript first presented at the 17th conference on Sustainable Development of Energy, Water and Environment Systems (SDEWES) held in Paphos, Cyprus, November 6th - 10th, 2022.

Abbreviations

a-CLR	Autothermal Chemical Looping Reforming
AR	Air Reactor
ASU	Air separation unit
ATR	Autothermal Reforming
BFB	Bubbling Fluidized Bed
CCS	Carbon Capture and Storage
CCU	Carbon Capture and Utilization
CHP	Combined Heat and Power
CLR	Chemical Looping Reforming
DFB	Dual Fluidized Bed
FB	Freeboard
FR	Fuel Reactor
OC	Oxygen Carrier
POM	Partial Methane Oxidation
SMR	Steam Methane Reforming
SR	Syngas H_2:CO Ratio
WGS	Water Gas Shift

References

[1] C. Da Costa Gomez, Biogas as an energy option: an overview, in: Woodhead Publishing (Ed.), Biogas Handb., Elsevier, 2013, pp. 1–16, https://doi.org/10.1533/9780857097415.1.
[2] O.W. Awe, Y. Zhao, A. Nzihou, D.P. Minh, N. Lyczko, A review of biogas utilisation, purification and upgrading technologies, Waste Biomass Valorizat. 8 (2017) 267–283, https://doi.org/10.1007/s12649-016-9826-4.
[3] P. Kaparaju, J. Rintala, 17 - generation of heat and power from biogas for stationary applications: boilers, gas engines and turbines, combined heat and power (CHP) plants and fuel cells, in: Woodhead Publ, Biogas Handb., 2013, pp. 404–427, https://doi.org/10.1533/9780857097415.3.404.
[4] E. Tomita, N. Kawahara, U. Azimov, Significance of biogas, its production and utilization in gas engines," biogas combustion engines for green energy generation, Biogas Combust. Engines Green Energy Gener. (2022) 1–12, https://doi.org/10.1007/978-3-030-94538-1_1.
[5] R. Kapoor, P. Ghosh, M. Kumar, V.K. Vijay, Evaluation of biogas upgrading technologies and future perspectives: a review, Environ. Sci. Pollut. Res. 26 (2019) 11631–11661, https://doi.org/10.1007/s11356-019-04767-1.
[6] S. O'Connor, E. Ehimen, S.C. Pillai, A. Black, D. Tormey, J. Bartlett, Biogas production from small-scale anaerobic digestion plants on European farms, Renew. Sustain. Energy Rev. 139 (2021), 110580, https://doi.org/10.1016/j.rser.2020.110580.
[7] P. Bareschino, E. Mancusi, C. Tregambi, F. Pepe, M. Urciuolo, P. Brachi, G. Ruoppolo, Integration of biomasses gasification and renewable-energies-driven water electrolysis for methane production, Energy 230 (2021), https://doi.org/10.1016/j.energy.2021.120863.
[8] A. Cabello, T. Mendiara, A. Abad, M.T. Izquierdo, F. García-Labiano, Production of hydrogen by chemical looping reforming of methane and biogas using a reactive and durable Cu-based oxygen carrier, Fuel 322 (2022), 124250, https://doi.org/10.1016/j.fuel.2022.124250.
[9] R. Soltani, M.A. Rosen, I. Dincer, Assessment of CO2 capture options from various points in steam methane reforming for hydrogen production, Int. J. Hydrogen Energy 39 (2014) 20266–20275, https://doi.org/10.1016/j.ijhydene.2014.09.161.
[10] M. Ortiz, A. Abad, L.F. de Diego, F. García-Labiano, P. Gayán, J. Adánez, Optimization of hydrogen production by Chemical-Looping auto-thermal Reforming working with Ni-based oxygen-carriers, Int. J. Hydrogen Energy 36 (2011) 9663–9672, https://doi.org/10.1016/j.ijhydene.2011.05.025.
[11] M. Tang, L. Xu, M. Fan, Progress in oxygen carrier development of methane-based chemical-looping reforming: a review, Appl. Energy 151 (2015) 143–156, https://doi.org/10.1016/j.apenergy.2015.04.017.
[12] J. Adanez, A. Abad, F. Garcia-Labiano, P. Gayan, L.F. De Diego, Progress in chemical-looping combustion and reforming technologies, Prog. Energy Combust. Sci. 38 (2012) 215–282, https://doi.org/10.1016/j.pecs.2011.09.001.
[13] T. Pröll, J. Bolhàr-Nordenkampf, P. Kolbitsch, H. Hofbauer, Syngas and a separate nitrogen/argon stream via chemical looping reforming – a 140kW pilot plant study, Fuel 89 (2010) 1249–1256, https://doi.org/10.1016/j.fuel.2009.09.033.
[14] M. Rydén, A. Lyngfelt, T. Mattisson, Synthesis gas generation by chemical-looping reforming in a continuously operating laboratory reactor, Fuel 85 (2006) 1631–1641, https://doi.org/10.1016/j.fuel.2006.02.004.
[15] M. Rydén, A. Lyngfelt, T. Mattisson, Chemical-looping combustion and chemical-looping reforming in a circulating fluidized-bed reactor using Ni-based oxygen carriers, Energy Fuel. 22 (2008) 2585–2597, https://doi.org/10.1021/ef800065m.
[16] M. Ortiz, L.F. de Diego, A. Abad, F. García-Labiano, P. Gayán, J. Adánez, Hydrogen production by auto-thermal chemical-looping reforming in a pressurized fluidized bed reactor using Ni-based oxygen carriers, Int. J. Hydrogen Energy 35 (2010) 151–160, https://doi.org/10.1016/j.ijhydene.2009.10.068.
[17] C. Song, W. Pan, Tri-reforming of methane: a novel concept for catalytic production of industrially useful synthesis gas with desired H2/CO ratios, Catal. Today 98 (2004) 463–484, https://doi.org/10.1016/j.cattod.2004.09.054.
[18] D. Pham Minh, T.J. Siang, D.-V.N. Vo, T.S. Phan, C. Ridart, A. Nzihou, D. Grouset, Hydrogen production from biogas reforming: an overview of steam reforming, dry reforming, dual reforming, and tri-reforming of methane, in: Hydrog. Supply Chain., Elsevier, 2018, pp. 111–166, https://doi.org/10.1016/B978-0-12-811197-0.00004-X.
[19] Ş. Özkara-Aydınoğlu, Thermodynamic equilibrium analysis of combined carbon dioxide reforming with steam reforming of methane to synthesis gas, Int. J. Hydrogen Energy 35 (2010) 12821–12828, https://doi.org/10.1016/j.ijhydene.2010.08.134.
[20] P. Cao, S. Adegbite, T. Wu, Thermodynamic equilibrium analysis of CO 2 reforming of methane: elimination of carbon deposition and adjustment of H 2/CO ratio, Energy Proc. 105 (2017) 1864–1869, https://doi.org/10.1016/j.egypro.2017.03.546.
[21] C. Jensen, M.S. Duyar, Thermodynamic analysis of dry reforming of methane for valorization of landfill gas and natural gas, Energy Technol. 9 (2021), 2100106, https://doi.org/10.1002/ente.202100106.
[22] A. Hoteit, M.K. Chandel, S. Durécu, A. Delebarre, Biogas combustion in a chemical looping fluidized bed reactor, Int. J. Greenh. Gas Control 3 (2009) 561–567, https://doi.org/10.1016/j.ijggc.2009.04.003.
[23] I. Adánez-Rubio, A. Nilsson, M.T. Izquierdo, T. Mendiara, A. Abad, J. Adánez, Cu-Mn oxygen carrier with improved mechanical resistance: analyzing performance under CLC and CLOU environments, Fuel Process. Technol. 217 (2021), 106819, https://doi.org/10.1016/j.fuproc.2021.106819.

[24] A. Cabello, T. Mendiara, A. Abad, J. Adánez, Techno-economic analysis of a chemical looping combustion process for biogas generated from livestock farming and agro-industrial waste, Energy Convers. Manag. 267 (2022), 115865, https://doi.org/10.1016/j.enconman.2022.115865.

[25] F. Kong, J. Swift, Q. Zhang, L.S. Fan, A. Tong, Biogas to H_2 conversion with CO_2 capture using chemical looping technology: process simulation and comparison to conventional reforming processes, Fuel 279 (2020), 118479, https://doi.org/10.1016/j.fuel.2020.118479.

[26] G. Diglio, P. Bareschino, R. Solimene, E. Mancusi, F. Pepe, P. Salatino, Numerical simulation of hydrogen production by chemical looping reforming in a dual fluidized bed reactor, Powder Technol. 316 (2017) 614–627, https://doi.org/10.1016/j.powtec.2016.12.051.

[27] I. Iliuta, R. Tahoces, G. Patience, Chemical-looping combustion process: kinetics and mathematical modeling, AIChE J. 56 (2010) 1063–1079, https://doi.org/10.1002/aic.

[28] G. Diglio, P. Bareschino, E. Mancusi, F. Pepe, Numerical assessment of the effects of carbon deposition and oxidation on chemical looping combustion in a packed-bed reactor, Chem. Eng. Sci. 160 (2017) 85–95, https://doi.org/10.1016/j.ces.2016.11.020.

[29] F.-X. Chiron, G.S. Patience, S. Rifflart, Hydrogen production through chemical looping using NiO/NiAl2O4 as oxygen carrier, Chem. Eng. Sci. 66 (2011) 6324–6330, https://doi.org/10.1016/j.ces.2011.03.060.

[30] L.F. de Diego, M. Ortiz, F. García-Labiano, J. Adánez, A. Abad, P. Gayán, Hydrogen production by chemical-looping reforming in a circulating fluidized bed reactor using Ni-based oxygen carriers, J. Power Sources 192 (2009) 27–34, https://doi.org/10.1016/j.jpowsour.2008.11.038.